Calculation of Three-Dimensional Viscous Flows in Turbomachinery with an Implicit Relaxation Method

C. Hah*
General Electric Company, Schenectady, New York

This study developed and appraised a numerical method for the complex three-dimensional compressible flow inside a cascade of airfoils at design and off-design conditions. The numerical method is based on an upwinding relaxation scheme with fully conservative control volume. The fully three-dimensional Reynolds-averaged Navier-Stokes equation is solved with an algebraic Reynolds stress model. The governing conservation equations and transport equations for turbulence quantities are solved sequentially. Comparison between the numerical solutions and experimental data indicates that various complex aerodynamic characteristics inside a cascade of airfoils are well represented with the numerical solutions.

Nomenclature

$C_s, C_1, C_\epsilon,$ $C_{\epsilon 1}, C_{\epsilon 2}, \gamma, D_6$	= constants in turbulence closure models
T	= mean temperature
c_p	= specific heat
D_{ij}	= diffusion coefficient in Eq. (9)
F_i	= additional body force in Eq. (2)
G_1, G_2, G_3	= convection coefficients in Eq. (9)
k	= turbulence kinetic energy
k_c	= thermal conductivity
P	$= -\overline{u_i u_j} U_{ij}$
p	= static pressure
R	= gas constant
β	= coefficient of thermal expansion
Ω_i	= angular velocity of rotor
δ_{ij}	= Kronecker delta
ϵ_{ijk}	= permutation tensor
ν	= kinematic viscosity
ρ	= density
θ	= dissipation due to viscosity [Eq. (3)]

Subscripts

p	= pressure side
s	= suction side
o	= total
1	= first node near the wall
w	= value at the wall
∞	= upstream condition

Superscripts

$(\bar{\ })$	= average value
$(\cdot)$	= with respect to relative system

Introduction

A RELIABLE analytical method for the complex three-dimensional flow is essential for the advanced design of modern gas turbine components. A realistic flow model that represents various important flow phenomena (three-dimensional shock pattern, shock/boundary-layer interaction, aerodynamic loss generation, etc.) will advance current design technology for a significant improvement in performance.

Recent experimental studies (e.g., Refs. 1 and 2) indicate that flow through a highly loaded modern compressor is extremely complicated. The flow is highly three-dimensional, involving shock/boundary-layer interaction and flow separation at design and off-design conditions. The effect of viscosity (thick suction surface boundary layer, shock-induced flow separation, etc.) significantly alters the flowfield, and flow models based on the inviscid assumption (potential or Euler solution) do not properly represent the shock location.

Several numerical approaches have been made to predict the flowfield more realistically. Denton[3] and Singh[4] added boundary-layer calculations along the solid walls to represent the viscous effects. Calvert[5] and Freeman[6] used the viscous-inviscid interaction method to represent strong coupling between the inviscid core flow and boundary layer. Although these methods provide reasonable solutions for certain types of transonic internal flows, further developments are necessary for a highly three-dimensional flow with the effects of viscosity not confined near the solid walls. Several studies based on compressible Navier-Stokes equations have been reported for two-dimensional cascade flows.[7-10] Solutions from these studies are very promising because they automatically capture shock location and because proper aerodynamic loss can be predicted if the proper physical model (turbulence modeling) is used. Currently, these methods are further expanded to get a stable solution for three-dimensional flows with reasonable cost.

The current study seeks to develop and appraise a numerical method for three-dimensional compressible flow inside a compressor rotor. The fully three-dimensional Reynolds-averaged Navier-Stokes equation for a steady state is solved to represent the flow inside a cascade of airfoils at design and off-design conditions. The current method is an extension of a numerical scheme which has been widely used for low-speed internal flows.[11] The method solves ρu_j, p, e, ρ, turbulence kinetic energy, and energy dissipation rates sequentially. The velocity, density, and pressure fields are closely coupled during the relaxation through multistage operator splitting. The method can be applied for the flowfield with a wide range of speed (from incompressible to supersonic flow regions). Additional transport equations (for example, 16 total transport equations for complex reacting flows) can be solved without major modification of the solution procedure. Such a versatility is often required when the flow attains different speed either in different regions or at different instants with a different set of dominant conservation equations. The method is based on a fully conservative control volume and a high-order upwinding is used to discretize convection terms.

Presented as Paper 86-0555 at the AIAA 24th Aerospace Sciences Meeting, Reno, NV, Jan. 6-9, 1986; received March 12, 1986; revision received Dec. 18, 1986.

*Fluid Mechanics Engineer, Corporate Research and Development. Member AIAA.

Previous studies[12-14] have indicated that a proper turbulence closure model is required to predict viscous flows at off-design conditions. The current viscous flow inside a cascade of airfoils contains flow separation, and the turbulence structure is significantly affected by the streamline curvature. An algebraic Reynolds stress model that was previously applied for the separated flow inside the cascade of airfoils[14] is used for the current study.

The numerical scheme with the above turbulence closure model is applied to the aerodynamic study of various cascades of airfoils at different flow conditions. Detailed three-dimensional flow structures are compared between the numerical solution and the experimental data.

Governing Equations

The differential equations used in this study are the Reynolds mass-averaged Navier-Stokes equations of a compressible fluid inside a rotating blade passage. Various conservation equations can be written using coordinates rotating with constant angular velocity (Ω_i):

$$\frac{\partial}{\partial x_i}(\rho U_i) = 0 \tag{1}$$

$$\frac{\partial}{\partial x_j}(\rho U_i U_j) + 2\rho\epsilon_{ijk}\Omega_j U_K = -\frac{\partial p}{\partial x_i} + \frac{\partial}{\partial x_j} \times \left[\mu\left(\frac{\partial U_i}{\partial x_j} + \frac{\partial U_j}{\partial x_i} - \frac{2}{3}\frac{\partial U_k}{\partial x_k}\delta_{ij}\right) - \rho\overline{u_i u_j}\right] + F_i \tag{2}$$

$$\frac{\partial}{\partial x_j}(\rho U_j e) = \frac{\partial}{\partial x_j}\left[\left(\frac{\mu}{Pr}\right)_{\text{eff}}\frac{\partial T}{\partial x_j}\right] - \frac{\partial}{\partial x_j}(pU_j) + U_i F_i + \frac{\partial}{\partial x_j}\left[U_i\mu\left(\frac{\partial U_i}{\partial x_j} + \frac{\partial U_j}{\partial x_i} - \frac{2}{3}\frac{\partial U_k}{\partial x_k}\delta_{ij}\right)\right] \tag{3}$$

$$P = \rho RT \tag{4}$$

where U_i = mean velocity, u_i = fluctuating velocity, e = total energy, Ω_i = angular velocity,

$$\left(\frac{\mu}{Pr}\right)_{\text{eff}} = \left(\frac{\mu}{Pr}\right)_{\text{laminar}} + \left(\frac{\mu}{Pr}\right)_{\text{turbulent}}$$

and $e = C_v T + \frac{1}{2}U_i U_i$. Detailed experimental studies on the transonic compressor rotor[1,2] indicate that shock/boundary-layer interaction induces flow separation, even at design conditions. An algebraic Reynolds stress model which was previously applied for the separated flow inside a cascade of airfoils[14] is further modified and used for the closure of the governing equations. The modification is to extend the previous model to the viscous sublayer region, which should be properly described for the flow inside very narrow tip clearance. Following studies by Lam and Bremhorst[15] and Rodi et al.,[16] rather simple modifications are made for the transport equations of turbulence kinetic energy and dissipation rate as follows:

$$\frac{\partial(\rho U_i k)}{\partial x_i} = \frac{\partial}{\partial x_i}\left(\frac{\mu_{\text{eff}}}{\sigma_K}\frac{\partial k}{\partial x_i}\right) - \rho\overline{u_i u_j}\,U_{ij} - \rho\epsilon \tag{5}$$

$$\frac{\partial(\rho U_i \epsilon)}{\partial x_i} = \frac{\partial}{\partial x_i}\left(\frac{\mu_{\text{eff}}}{\sigma\epsilon}\frac{\partial \epsilon}{\partial x_i}\right) + C_s\frac{\rho\epsilon^2}{k^3}(\overline{u_i u_j} - 2/3\,k\delta_{ij})(\overline{u_j u_i} - 2/3k\delta_{ji}) - C_R\rho f_\epsilon l\frac{\epsilon}{k}\overline{u_i u_j}U_{ij} - C_{\epsilon 2}\rho f_{\epsilon 2}\frac{\epsilon^2}{k} \tag{6}$$

where

$$\mu_{\text{eff}} = \mu + C_\mu f_\mu \rho k^2/\epsilon;\ k = \tfrac{1}{2}\delta_{ij}\overline{u_i u_j}$$

$$f_\mu = (1 - e^{-A_\mu R_1})^2\left(1 + \frac{A_t}{R_t}\right);\ f_{\epsilon 1} = 1 + \left(\frac{A_c}{f_\mu}\right)^3$$

$$f_{\epsilon 2} = 1 - e^{-R_t^2}$$

$$R_1 = \sqrt{k}l/\nu$$

$$R_t = k^2/\nu\epsilon$$

and l is the distance between the node and the nearest solid surface.

The Reynolds stress components in the momentum equations are estimated with the following algebraic equations:

$$0 = (1 + C_1)(-\overline{u_k u_j}U_{i,k} - \overline{u_k u_i}U_{j,k})(1 - \gamma) - 2(\epsilon_{ilm}\Omega_l\overline{u_m u_j} + \epsilon_{jlm}\Omega_l\overline{u_m u_i}) - 2/3\delta_{ij}(1 - \gamma)\epsilon - C_{\phi 1}(\epsilon/k)(\overline{u_i u_j} - 2/3\delta_{ij}) + D_6\Omega_n(\epsilon_{lnj}\overline{u_l u_j} + \epsilon_{lnj}\overline{u_l u_i}) \tag{7}$$

where γ and $C_{\phi 1}$ are constants in the modeling and C_1 is a variable that represents the collective effects of the convection and the diffusion terms in the exact transportation equations of the Reynolds stresses.

Equations (5-7) have been used previously for various subsonic flows with strong secondary flows and flow separation.[17] Various constants in the turbulence modeling are not optimized for the present study. The values are as follows:

$$C_\mu = 0.09,\ C_{\phi 1} = 1.5,\ C_s = 1.8,\ C_{\epsilon 2} = 1.44,\ D_6 = 0.7$$

$$\delta_k = 1.0,\ \delta_\epsilon = 1.22,\ \gamma = 0.6,\ C_R = 0.46,\ A_\mu = 0.016$$

$$A_t = 19.5,\ A_{c1} = 0.06$$

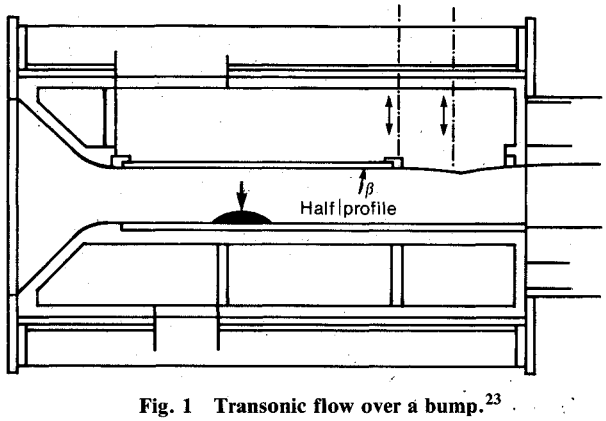

Fig. 1 Transonic flow over a bump.[23]

Numerical Procedure

The numerical solution of Eqs. (1-7) for the turbulent flow inside a real compressor rotor remains a formidable task although the latest generation of supercomputers has allowed significant development in the basic computational fluid mechanics.[18-20] The additional body forces (centrifugal and Coriolis) from the system rotation and inherent complex boundary conditions (periodicity, tip-leakage flows treatment) make the overall numerical system very stiff.

The current numerical scheme is an extension of the previously developed method for subsonic viscous flows inside blade rows.[11] With the original scheme for low-speed flow, the pressure is used as a major dependent variable instead of density. This is because the linkage between pressure and density weakens in the low Mach number range. As the governing equations are solved sequentially, each corresponding finite-difference equation should be represented with a diagonally dominant matrix. For this purpose, the continuity and the momentum conservation equations are combined for the pressure equation. The effect of density change during pressure calculation is handled indirectly by operator splitting.[22] This rather explicit treatment of density during relaxation provides reasonably efficient solution for most medium-speed subsonic flows. However, significant under-relaxation of density is required with this procedure when applied for high Mach number flow. This is because the single pressure equation is used to correct both velocity and density field in addition to pressure field, and this approach becomes inefficient when density varies significantly. For the current study, the main dependent variables are chosen as ρU_i, p, and e instead of U_i, p, and e. With the new dependent variables, the pressure equation is used to correct only one variable, Cartesian momentum (ρU_i), instead of two variables U_i and ρ. This set of dependent variables is mainly to maintain better coupling between dependent variables during the relaxation and to avoid extreme under-relaxation of density. For the convenience of formulation, the governing momentum equations are rewritten in the following form in the Cartesian system:

$$\frac{\partial}{\partial x}(U\phi)+\frac{\partial}{\partial y}(V\phi)+\frac{\partial}{\partial z}(W\phi)=\frac{\partial}{\partial x}\left(\frac{\Gamma_\phi}{\rho}\frac{\partial\phi}{\partial x}\right)+\frac{\partial}{\partial y}\left(\frac{\Gamma_\phi}{\rho}\frac{\partial\phi}{\partial y}\right)+\frac{\partial}{\partial z}\left(\frac{\Gamma_\phi}{\rho}\frac{\partial\phi}{\partial z}\right)+S_\phi \tag{8}$$

where ϕ is any dependent variable (ρU, ρV, ρW). To express the governing equations as Eq. (8), several diffusion terms are divided into implicit and explicit parts. For example,

$$\frac{\partial}{\partial x_j}\left(\mu_{\text{eff}}\frac{\partial U_i}{\partial x_j}\right)=\frac{\partial}{\partial x_j}\left[\frac{\mu_{\text{eff}}}{\rho}\frac{\partial(\rho U_i)}{\partial x_j}-\frac{\mu_{\text{eff}}}{\rho}U_i\frac{\partial\rho}{\partial x_j}\right]$$

and the first part is handled implicitly while the second part is included as a part of the source term (S_ϕ). Equation (8) is identical with the original governing equations.

Several diffusion terms are regrouped for the convenience of numerical solution. Both the effective diffusion coefficient Γ_ϕ and density are updated with the values at previous relaxation and used to compute the new diffusion fluxes at the control volume surface. The numerical representation of the source term (S_ϕ) is done consistently with other terms. On the transformed curvilinear coordinates (ξ,η,ψ), the following form of a similar equation can be written:

$$\begin{aligned}&\frac{1}{J}\frac{\partial}{\partial\xi}(G_1\phi)+\frac{1}{J}\frac{\partial}{\partial\eta}(G_2\phi)+\frac{1}{J}\frac{\partial}{\partial\psi}(G_3\phi)\\&=\frac{1}{J}\frac{\partial}{\partial\xi}\left[\frac{\Gamma'_\phi}{J}D_{\xi\xi}\phi_\xi+\frac{\Gamma'_\phi}{J}D_{\xi\eta}\phi_\eta+\frac{\Gamma'_\phi}{J}D_{\xi\psi}\phi_\Psi\right]\\&+\frac{1}{J}\frac{\partial}{\partial\eta}\left[\frac{\Gamma'_\phi}{J}D_{\eta\xi}\phi_\xi+\frac{\Gamma'_\phi}{J}D_{\eta\eta}\phi_\eta+\frac{\Gamma'_\phi}{J}D_{\eta\psi}\phi_\Psi\right]\\&=\frac{1}{J}\frac{\partial}{\partial\psi}\left[\frac{\Gamma'_\phi}{J}D_{\psi\xi\phi\xi}+\frac{\Gamma'_\phi}{J}D_{\psi\eta}\phi_\eta+\frac{\Gamma'_\phi}{J}D_{\psi\psi}\phi_\Psi\right]+S_\phi\end{aligned} \tag{9}$$

where $\Gamma'_\phi=\Gamma_\phi/\rho$.

The system of Eq. (9) can be solved in various ways. For steady flow problems, pseudo-time accurate or relaxation-type approaches can be used for a fast solution. The system can be solved as a block variable, or a sequential type of approach can be used for an open system of equations (additional conservation equations for turbulence or other conservation equations for reacting flows). With the divergence theorem, Eq. (9) can be written for arbitrarily shaped control volume

$$\int_A \phi^{n+1}G_i n_i\,dA=\int_A\frac{\Gamma'_{\text{eff}}}{E_{ij}}\phi_i^{n+1}n_j\,dA+\int_R S_\phi\,dR \tag{10}$$

Various terms in Eq. (9) are integrated numerically for arbitrarily shaped control volumes to get finite-difference equations for the unknowns at the computational nodes.

For the discretization of the convection term, a hybrid scheme that combines the central differencing, the quadratic interpolation scheme,[21] and skew upwinding scheme is used. When the central differencing of the convection term violates stability criteria (i.e., when the cell Peclet number exceeds 2), a modified quadratic interpolation scheme is used along the streamline. As the quadratic interpolation scheme becomes unstable when the cell Peclet number exceeds critical value (which is between 4 and 8, depending on local flow-to-grid skewness, a second-order accurate upwinding is used along the streamline. Dependent variables at up to 125 surrounding nodes can be related for the finite-difference formulation. However, unknown values at 27 surrounding nodes are handled implicitly and the influence of other nodes, which is a lower order of magnitude because of the boundedness of the upwinding, is handled explicitly. Second-order accurate central differencing is used for the diffusion terms. The overall scheme is of second-order accuracy in the physical domain and no additional artificial viscosity is added for stability of solution. The resulting system of linear algebraic equation is solved with successive over-relaxation. At each iteration, the equations are solved in blade-to-blade plane, through-flow plane, and cross-flow plane in alternating order.

The concept of pressure-implicit split operator by Issa[22] is modified for the current scheme and extended for three-dimensional general geometries. With each iteration step, one prediction step and two correction steps are used for the new values of ρU, ρV, ρW, and P. The gas state equation is used to calculate ρ, U_i from ρU_i, e, and P. The prediction step for the $(\rho U)_i$ is as follows:

$$A_p(\rho U)_i^*=\Sigma A_{pm}(\rho U)_{im}^*-\Delta_i p^n+S_i \tag{11}$$

where * denotes intermediate value at this step, A_p and A_{pm} are the finite-difference coefficients, and n represents the value at the nth iteration. As the above prediction step is based on the pressure field at previous iteration, the resulting $(\rho U_i)^*$ do not satisfy mass conservation. Two correction steps are to obtain $(\rho U_i)^{n+1}$, ρ^{n+1} which satisfy finite-difference equations for momentum and mass conservation.

$$A_p(\rho U)_i^{n+1}=\Sigma A_{pm}(\rho U)_{im}^{n+1}-\Delta_i p^{n+1}+S_i \tag{12}$$

By combining Eqs. (11) and (12)

$$(\rho U_i)^{n+1}-(\rho U_i)^*=A_p^{-1}[\Sigma A_{pm}(\rho U)_{im}^{n+1}-\Sigma A_{pm}(\rho U)_{im}^*]-A_p^{-1}\Delta_i(p^{n+1}-p^n) \tag{13}$$

The implicit equation (13) cannot be solved in a single step because of the implicit terms (first term on the right-hand side). The first correction step is formed by neglecting effects of convection terms in Eq. (13)

$$(\rho U_i)^{**}-(\rho U_i)^*=A_p^{-1}\Delta_i(p^*-p^n) \tag{14}$$

With the following conservation condition

$$\Delta_i(\rho U_i)^{**}=0 \tag{15}$$

a Poisson-like equation is solved for p^*-p^n.

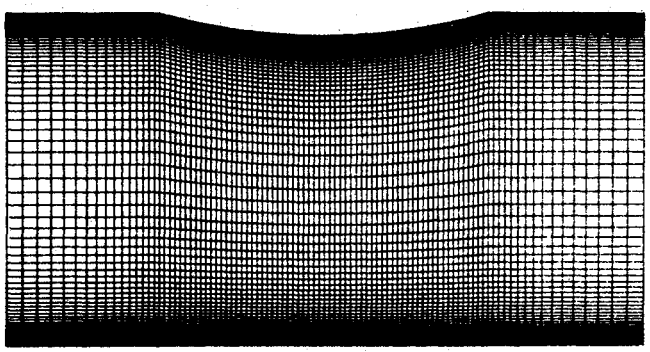

Fig. 2 computational grid.

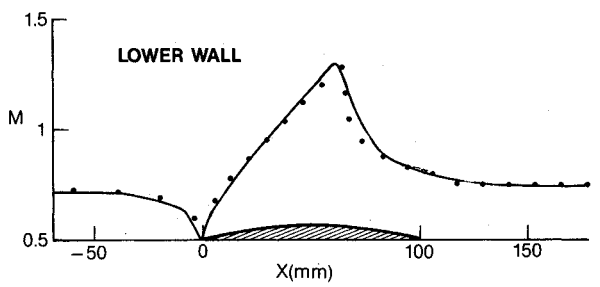

Fig. 3a Comparison of wall static pressure on the upper wall (•: measurement[23], -: calculation).

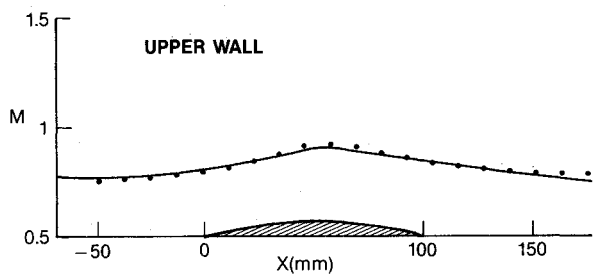

Fig. 3b Comparison of wall static pressure on the lower wall (•: measurement[23], -: calculation).

Then $(\rho U_i)^{**}$ is obtained by Eq. (14). The second correction step is to include the effects of convection terms in Eq. (13).

$$(\rho U_i)^{n+1} - (\rho U_i)^{**} = A_p^{-1} \Sigma A_{pm} [(\rho U)^{**} - (\rho U)^*] - \Delta_i (p^{n+1} - p^*)$$

Again, $\Delta_i (\rho U_i)^{n+1} = \Delta_i (\rho U_i)^{**} = 0$. During the entire prediction and correction step, the coefficients A_p and A_{pm} are frozen with the value at step n. Inside the supersonic flow region, where the "domains of dependence" can be used for numerical purposes, the grid nodes are shifted upstream for the pressure calculation, and fluxes at the control volume surfaces are calculated with the variables in the domain of dependence. As the utilized discretization of convection term essentially assures upwinding of ρU_i, this additional shifting of the pressure field prevents downstream variables from influencing upstream conditions in supersonic flow regions. Single implicit steps for e, k, and ϵ follow after the above multiple steps.

Computational Grid and Boundary Condition

H-type grids are used for the current problem with proper modification near the blade surface and the leading edge. A staggered grid system is used with the control volume approach. The control volume surface of the scalar node lies along the solid wall boundary, and fluxes of mass and momentum across these surfaces are set to zero along with the no-slip condition. The first node is typically located 0.0005 chord length away from the blade surface. The static pressure on the solid wall surface is obtained through the extrapolation of interior values.

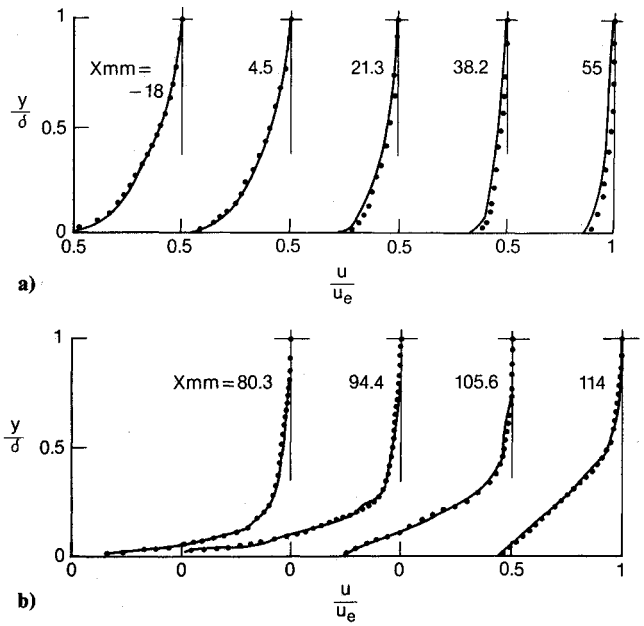

Fig. 4 Comparison of boundary-layer velocity profiles. a) upstream from the shock wave; b) downstream from the shock wave.

At the outflow boundary, the static pressure is held with a given value at one point and asymptotic conditions are used for other dependent variables. No additional radial momentum equation is solved at the exit for boundary condition because the pressure equation is solved fully implicitly with the current scheme. The repeating periodicity conditions are explicitly imposed upstream and downstream of the blade. At the inflow boundary, the total pressure, the total temperature, and inlet flow angles are fixed with the experimental value and the static pressure is extrapolated. For the turbulence quantities, a fixed value of turbulence kinetic energy is used and characteristic length scale (0.1% of pitch at midspan) is used for dissipation rate at inlet. Residuals of finite-difference equations are monitored at each computational plane. When all these residuals are less than 10^{-4} of inlet flow quantities, the solution is assumed to be converged. The detailed Mach number contour, local quantities (turning angle, mass-averaged total temperature, etc.) do not change with the current computational grid after the residual is lower than 10^{-3}. The necessary CPU per grid is about 2×10^{-3} s for each iteration on the Cray XMP.

Transonic Flow over a Bump

The current numerical scheme has been tested for compressible flows over a bump on a channel wall at various flow conditions. The experimental data by Delery et al.[23] are used for verification purposes. The test geometry is shown in Fig. 1. The experiments were carried out in a bidimensional transonic nozzle (cross section 100×120 mm). A circular bump with maximum thickness of 7% is mounted on the nozzle lower wall. The boundary layer near the leading edge of the bump is fully turbulent and has a physical thickness close to 5 mm.

Although the reported results are very close to a two-dimensional nature, the flow was calculated as a three-dimensional one. A computational grid of $104 \times 68 \times 11$ in streamwise, normal, and spanwise directions with exponential

stretching in normal direction is used (Fig. 2). The first node was located 0.0005 chord length away from the wall. The solution was converged with 550 iterations and about 25 min of CPU on a Cray XMP. Comparisons between measurement and calculation are made for configuration 3 in an experimental study which shows significant shock/boundary-layer interaction with detailed profile measurements. The corresponding freestream Mach number is 0.71 and Reynolds number, based on the chord length, is 1.54×10^6. The static pressure distribution on the walls is compared in Fig. 3 in terms of corresponding Mach number. Comparisons in Fig. 3 indicate that the overall flowfield is very well predicted with the current method. The development of wall boundary layer is compared in Fig. 4. The strong distortion of the boundary layer due to strong pressure gradient upstream of the shock is also well predicted. Characteristic values of the boundary layer are compared in Fig. 5.

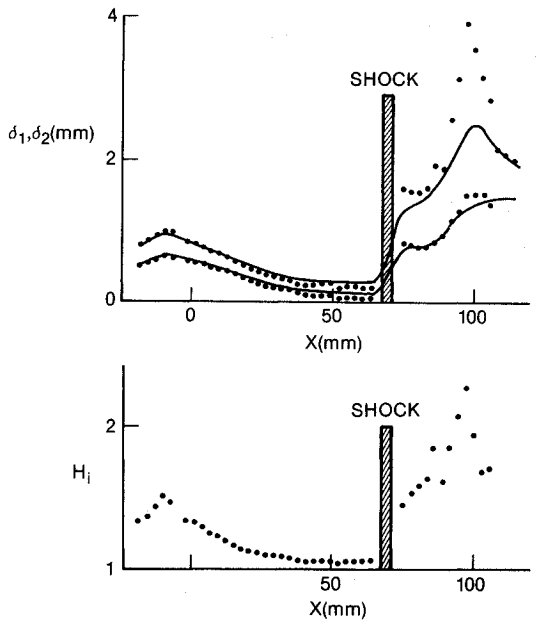

Fig. 5 Comparison of characteristic values of boundary layer.

Comparison of a Compressor Rotor Flow

The experimental data from a transonic compressor rotor by Dunker and Hungenberg[2] were used for the purpose of verification and appraisal. The test compressor was a single-stage transonic axial compressor without inlet guide vanes. The design pressure ratio was 1.51 and the mass flow rate was 17.3 kg/s at 20,260 rpm with 28 rotor blades. Further details of the compressor can be found in Ref. 24. The detailed measurements were performed with a conventional probe and an L2F laser velocimeter. The compressor flow path and overall performance map are shown in Fig. 6. The numerical calculations were made at three flow rates (choke, maximum efficiency, and near surge) at 100% of design speed. The computational grid shown in Fig. 7 has 62 axial stations, 35 blade-to-blade stations, and 24 spanwise stations. The first node along the blade-to-blade direction was located 0.001 chord length away from the blade surface. As no detailed information about blade tip is available and no measurements are reported near the endwalls, no spanwise clustering is used. The overall grid size was compromised because of the overall storage limitation and available CPUs of the computer. The solution was obtained with about 700 iterations and 35 min of CPU on a Cray XMP.

Mean Flowfield

Figure 8 shows comparison of the mean flowfield at 68% blade height when the compressor throttle is open (choke margin). The experimental data indicate a very complex flowfield: an attached shock wave at the blade leading edge, an oblique shock within the blade passage and a consequent separation bubble on the suction surface (about 70% chord), and a normal shock on the suction surface trailing edge. The numerical solution based on the current computational grid shows all these complex phenomena well. The flowfields at maximum efficiency (which is obtained by increasing the back pressure slightly) are compared in Fig. 9. As the mass flow rate reduces, the normal shock near the trailing edge at the choke condition is moved up near the leading edge. A bow shock is formed ahead of the leading edge and a λ shock is formed around 50% chord on the suction surface. The movement of the normal shock from the trailing edge to the leading edge is due to the increased viscous blockage inside the blade passage. For this flow condition, inviscid calculation predicts shock location near the trailing edge (dotted line in Fig. 9) because the decrease of effective blade passage area due to viscous effect is not properly calculated. The current numerical results

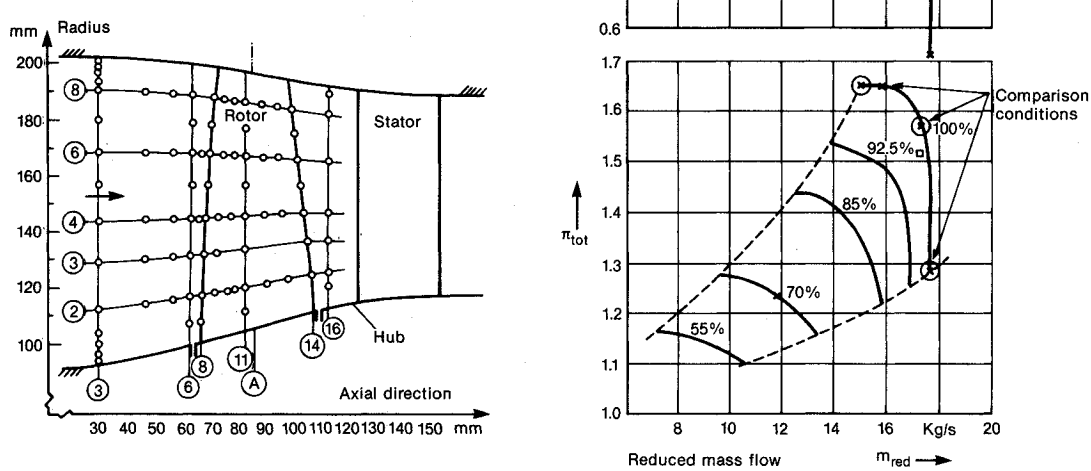

Fig. 6 compressor flow path and overall performance map.[2]

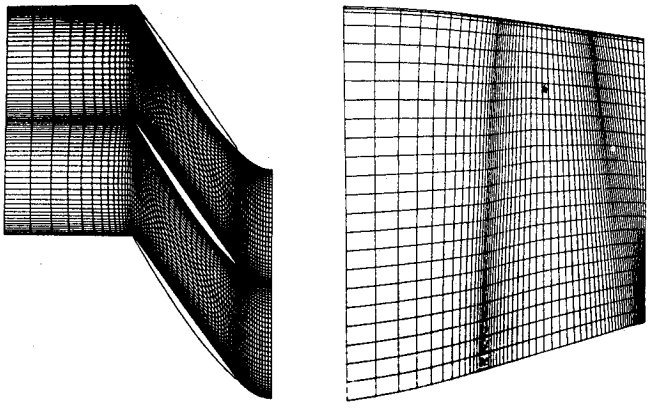

Fig. 7 Computational grid for an isolated transonic rotor.

show the change of flowfield due to the reduced mass flow rate very well. However, the detailed structure of the λ shock is not well presented. The presence of the λ shock is a very complicated viscous phenomena with small length scales dominating; the accurate prediction of this phenomena requires a very fine grid along with correct representation of viscous shear stresses. Detailed flowfields near surge conditions are compared in Fig. 10. A detached normal shock is formed at the blade passage entrance because of a high positive incidence angle and a subsonic bubble appears around the blade leading edge. The experimental data further indicate the formation of a λ shock and a boundary-layer layer separation. The numerical results accurately represent the overall flowfield at this high positive incidence angle. The Mach number contour also indicates that the boundary-layer separation and the overall flow diffusion are well predicted.

Detailed mean flowfields inside a transonic compressor rotor were compared at three different flow conditions. Also,

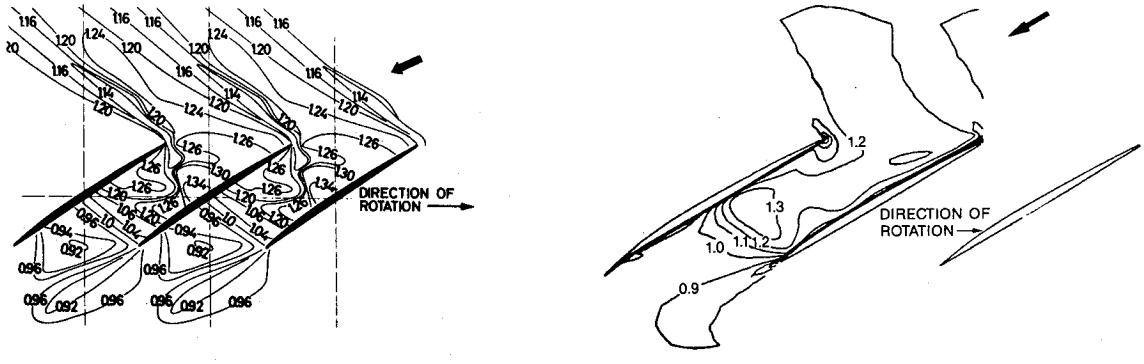

Fig. 8 Comparison of relative Mach number contours on rotor blade section at 68% blade height, 100% speed, choke margin, $m = 17.6$ kg/s.

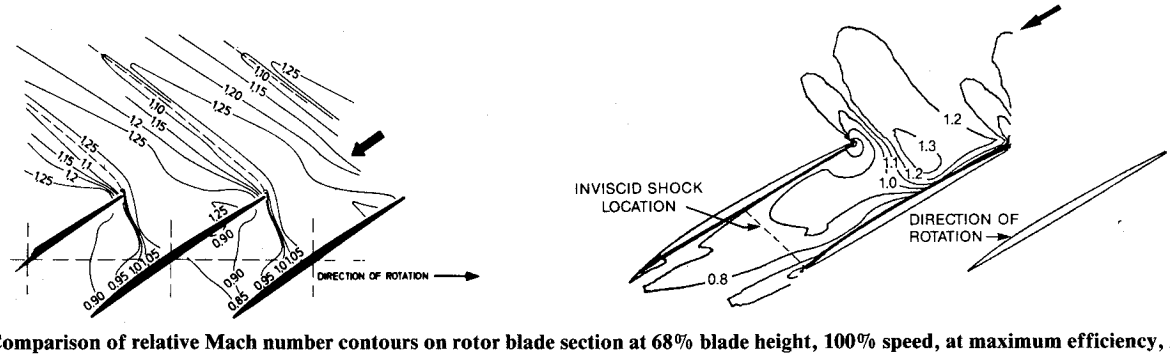

Fig. 9 Comparison of relative Mach number contours on rotor blade section at 68% blade height, 100% speed, at maximum efficiency, $m = 17.15$ kg/s.

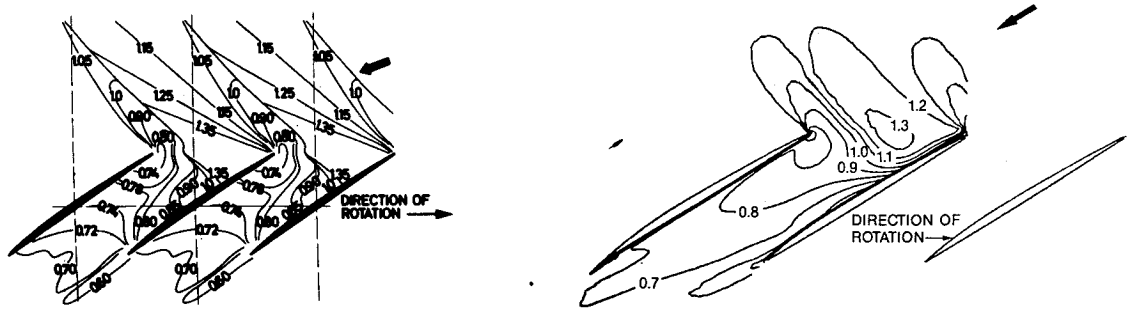

Fig. 10 Comparison of relative Mach number contours on rotor blade section at 68% blade height, 100% speed, at 1.5% off compressor surge, $m = 15.35$ kg/s.

three-dimensional flow structures were compared at typical flow conditions. With the applied computational grid and turbulence closure, the overall qualitative picture of the flow is well predicted. Further, details of the field (λ-shock, detailed flow separation) can be resolved with finer computational grid.

Relative Flow Angle

The axial chordwise distributions of the relative flow angle through the rotor at three different flow conditions are compared in Fig. 11. The comparisons are made at 10% of blade pitch off the suction surface, at the midchannel, and at 10% of blade pitch off the pressure surface. Also, the metal angles of the blade suction, the pressure surface, and the centerline are given for comparison (solid line without symbol). The experimental data again show the various complex effects of shock/boundary-layer interaction and flow separation. Near the suction surface, the flow angle changes because of the impinging of the normal shock. The location of these changes of angle depends on the flow rate (25% chord at surge and 45% at maximum efficiency). Also, the real flow turning at the midchannel is quite different from the design camber line angle. Here again, the numerical results predict the local mean flow angle reasonably well. The detailed change of flow turning due to shock/boundary-layer interaction and separation of the boundary layer is sufficiently well predicted to be utilized

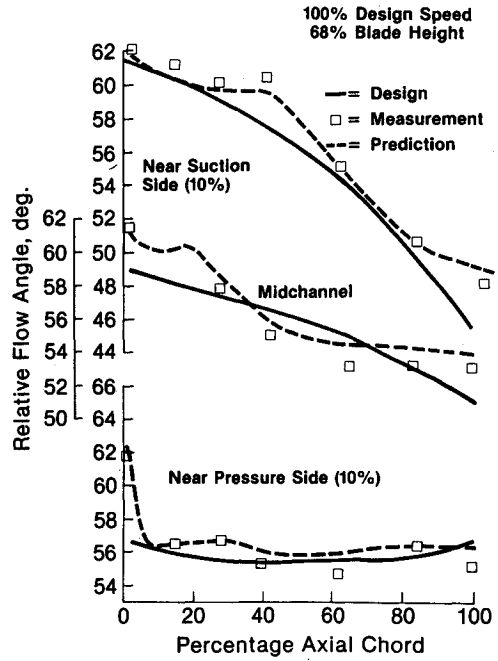

Fig. 11b Comparison of relative flow angle distribution at maximum efficiency ($m = 17.15$ kg/s).

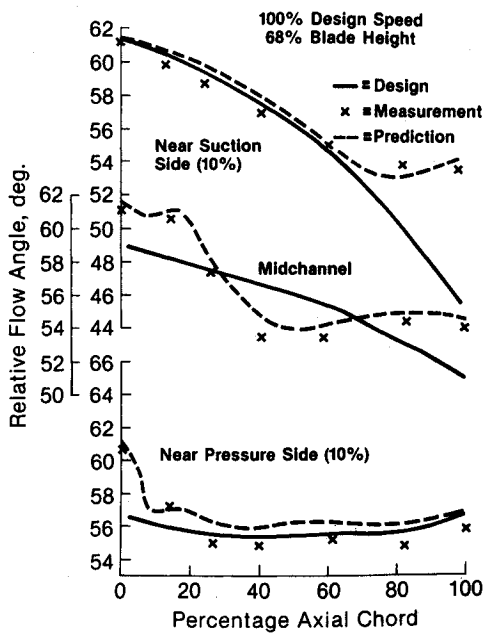

Fig. 11a Comparison of relative flow angle distribution at choke margin ($m = 17.6$ kg/s).

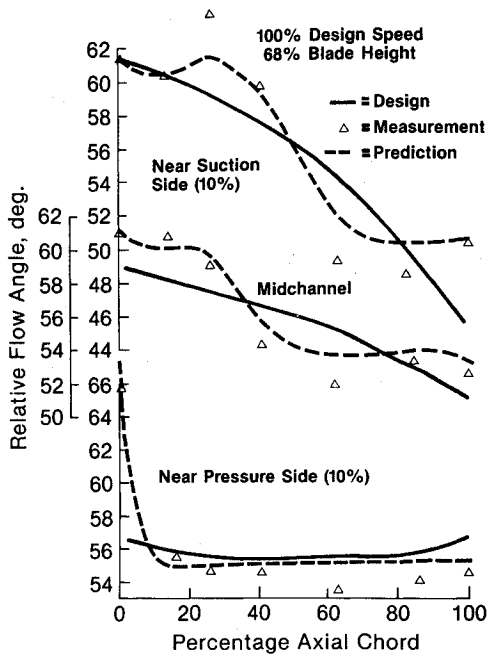

Fig. 11c Comparison of relative flow angle distribution at 1.5% off surge ($m = 15.35$ kg/s).

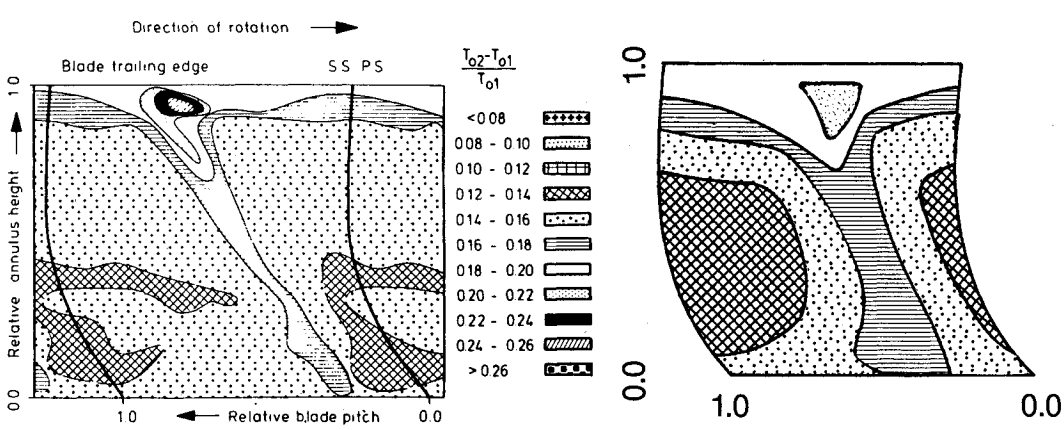

Fig. 12 Comparison of total temperature rise at maximum efficiency ($m = 17.15$ kg/s).

for blade passage design. Again, the extent of flow separation is underpredicted, probably because of insufficient grid resolution for the small-length scale phenomena. Like relative Mach number contours, the inviscid calculation does not predict relative flow angles properly. The predicted inviscid flow angles are similar to the blade metal angles, and this is again because the development of the viscous boundary layer is not modeled adequately.

Total Temperature Rise

The total temperature rise through the rotor at maximum efficiency is compared in Fig. 12. The comparison is made at station 16 in Fig. 6. The region of high-energy input clearly marks the blade wake. Because of the different actual distances from the blade trailing edge at hub and tip, the wake is shifted against the rotating distance. The numerical solution clearly shows the increase of enthalpy rise toward the blade tip and a higher temperature rise in the blade wake. Clearly, the numerical prediction reproduces three-dimensional flow nature reasonably well. Obviously, improvement in the quantitative aspect of the solution can be achieved through refined computational grids.

Summary

The current design technology, which is based mainly on an empirical correlation, can already produce quite efficient gas turbine components. To achieve further major improvements, the details of the flow should be more precisely understood and modeled. The current study is to provide such a tool for advanced gas turbine design.

A numerical scheme was developed for three-dimensional compressible turbulent flow inside a cascade of airfoils. The method solves governing conservation equations (continuity, momentum, energy, and turbulence transport) sequentially and additional equations (for example, additional equations for reacting flow) can be added without major modification of the code. The method uses a higher-order upwinding relaxation scheme for a stable steady-state solution. An algebraic Reynolds stress model was used for the turbulence closure.

Detailed experimental data of a transonic flow over a bump inside a channel were used for validation purposes. Also, the method has been applied to predict three-dimensional flows inside a highly loaded compressor rotor. The comparison between the measurement and the calculation indicates that the numerical scheme predicts various complex flow phenomena properly. The current scheme can be efficiently used for a flow with a wide range of flow regimes (low-subsonic to transonic flow). However, more significant effort is needed for further improvement of the turbulence closure model and for further reduction of required computer resources.

References

[1]Strazisar, A. J., "Investigation of Flow Phenomena in Transonic Fan Rotor Using Laser Anemometry," ASME Paper 84-GT, 199, 1984.

[2]Dunker, R. J. and Hungenberg, H. G., "Transonic Axial Compressor Using Laser Anemometry and Unsteady Pressure Measurements," *AIAA Journal*, Vol. 18, Aug. 1980, pp. 973–979.

[3]Denton, J. D., Lecture Notes, ASME Turbomachinery Institute Course on Fluid Dynamics of Turbomachinery, July 18–27, 1983.

[4]Singh, U. K., "A Computation and Comparison with Measurements of Transonic Flow in an Axial Compressor Stage with Shock and Boundary Layer Interaction," *ASME Journal of Engineering for Power*, Vol. 104, April 1982, pp. 510–515.

[5]Calvert, W. J., "Application of an Inviscid-Viscous Interaction Method to Transonic Compressor Cascades," NGTE Rept. R 83001, March 1983.

[6]Freeman, C., "A Viscous Inviscid Interaction Method for Calculating the Flow in Transonic Fan Blade Passages by the Use of a Time-Dependent Free Stream Calculation and a Time-Dependent Boundary Layer Calculation," *International Mechanical Engineering Conference, Computational Methods in Turbomachinery*, Birmingham, U. K., April 1984.

[7]Steger, J. L., Pullman, T. H., and Chima, R. V., "An Implicit Finite Difference Code for Inviscid and Viscous Cascade Flow," AIAA Paper 80-1427, 1980.

[8]Shamroth, S., Giveling, H. J., and McDonald, H., "A Navier-Stokes Solution for Laminar and Turbulent Flow Through a Cascade of Airfoils," AIAA Paper 80-1426, 1980.

[9]Thompkins, W. T. Jr., Tong, S. S., Bush, R. H., Usab, W. J. Jr., and Norton, R. J. G., "Solution Procedures for Accurate Numerical Simulations of Flow in Turbomachineary Cascades," AIAA Paper 83-0257, 1983.

[10]Dawes, W. N., "Computation of Off-Design Flows in a Transonic Compressor Rotor," ASME Paper 85-GT-1, 1985.

[11]Hah, C., "A Navier-Stokes Analysis of Three-Dimensional Turbulent Flows Inside Turbine Blade Rows at Design and Off-Design Conditions," *ASME Journal of Engineering for Power*, Vol. 106, April 1984, pp. 421–429.

[12]Leschziner, M. A. and Rodi, W., "Calculation of Annular and Twin Parallel Jets Using Various Discretization Schemes and Turbulence Model Variations," *ASME Journal of Fluids Engineering*, Vol. 103, June 1981, pp. 352–360.

[13]Hah, C., "Calculation of Planar, Conical and Annular Diffuser Flows with Inlet Swirl and Inlet Distortion Effects," *AIAA Journal*, Vol. 21, Aug. 1983, pp. 1127–1133.

[14]Hah, C., "Modeling of Turbulent Flow Fields through Cascade of Airfoils at Stall Condition," *AIAA Journal*, Vol. 23, Sept. 1985, pp. 1411–1417.

[15]Lam, C. K. G. and Bermhorst, K. A., "Modified Form of the $k\epsilon$ Model for Predicting Wall Turbulence," *Journal of Fluids Engineering*, Vol. 103, June 1981, p. 456.

[16]Rodi, W., Celik, I., Demuren, A. O., Scheuerer, G., Shirani, I., Leschziner, M. A., and Rastogi, A. K., *Proceedings of 1980-81 AFOSR-HTTM Stanford Conference on Complex Turbulent Flows*, edited by S. J. Kline, B. J. Cantwell, and G. M. Lilley, Vol. III, 1982, p. 1495.

[17]Hah, C., "A Numerical Modeling of Endwall and Tip-Clearance Flow of an Isolated Compressor Rotor," *Journal of Engineering for Gas Turbines and Power*, Jan. 1986, Vol. 108, pp. 15–21.

[18]Briley, W. R. and McDonald, H., "Solution of the Three-Dimensional Compressible Navier-Stokes Equations by an Implicit Technique," *Proceedings of the 4th International Conference on Numerical Methods in Fluid Dynamics*, Vol. 35, pp. 105–110, New York, Springer, 1975 (see also United Aircraft Research Laboratory Rept. M911363-6, 1973).

[19]Beam, R. M. and Warming, R. F., "An Implicit Finite-Difference Algorithm for Hyperbolic Systems in Conservation Law Form," *Journal of Computational Physics*, Vol. 22, pp. 87–110, Jan. 1976.

[20]MacCormack, R. W., "Current Status of Numerical Solutions of the Navier-Stokes Equations," AIAA Paper 85-0032, 1985.

[21]Leonard, B. P., "A Stable and Accurate Convective Modeling Procedure Based on Quadratic Upstream Interpolation," *Computer Methods in Applied Mechanics and Engineering*, Vol. 19, Jan. 1979, pp. 59–98.

[22]Issa, R. I., "Solution of Implicity Discretized Fluid Flow Equations by Operator-Splitting," Internal Report, Department of Mineral Resources Engineering, Imperial College, London, 1982.

[23]Delery, J., Chattot, J. J., and Le Balleur, J. C., "Viscous Interaction with Separation in Transonic Flow," AGARD-CP-168, Nov. 1975.

[24]Strinning, P. E. and Dunker, R. J., "Aerodynamische und Schaufelauslegung einer Transsonischen Axialverdichterstufe," *Forschungsbericht Verbrennungskraftmaschinen*, Heft 178, 1975.